

# Development of Hub Corner Stall and Its Influence on the Performance of Axial Compressor Blade Rows

C. Hah

NASA Lewis Research Center,  
Cleveland, OH 44135

J. Loellbach

ICOMP/NASA Lewis Research Center,  
Cleveland, OH 44135

A detailed investigation has been performed to study hub corner stall phenomena in compressor blade rows. Three-dimensional flows in a subsonic annular compressor stator and in a transonic compressor rotor have been analyzed numerically by solving the Reynolds-averaged Navier-Stokes equations. The numerical results and the existing experimental data are interrogated to understand the mechanism of compressor hub corner stall. Both the measurements and the numerical solutions for the stator indicate that a strong twisterlike vortex is formed near the rear part of the blade suction surface. Low-momentum fluid inside the hub boundary layer is transported toward the suction side of the blade by this vortex. On the blade suction surface near the hub, this vortex forces fluid to move against the main flow direction and a limiting stream surface is formed near the hub. The formation of this vortex is the main mechanism of hub corner stall. When the aerodynamic loading is increased, the vortex initiates further upstream, which results in a larger corner stall region. For the transonic compressor rotor studied in this paper, the numerical solution indicates that a mild hub corner stall exists at 100 percent rotor speed. The hub corner stall, however, disappears at the reduced blade loading, which occurs at 60 percent rotor design speed. The present study demonstrates that hub corner stall is caused by a three-dimensional vortex system and that it does not seem to be correlated with a simple diffusion factor for the blade row.

## Introduction

Design trends for modern multistage compressors continue to increase blade loadings and decrease aspect ratios. Sophisticated design tools are required to account for the increased complexity of the resulting flow fields. During the last decade, numerical methods based on the Reynolds-averaged Navier-Stokes equations have made remarkable progress in turbomachinery design applications. Currently, steady and unsteady three-dimensional viscous flow calculations are routinely performed during the design cycle.

Although various CFD codes have been successfully applied to turbomachinery component design, further advances in numerics as well as physical modeling should be pursued. During the 1994 ASME/IGTI-sponsored CFD validation exercise (see Strazisar and Denton, 1995), many questions were raised concerning widely scattered blind CFD predictions. One of the issues was whether the current generation of CFD codes can calculate compressor hub corner stall. The importance of accurate calculations of endwall flows for multistage compressor designs has been pointed out by previous studies (Adamczyk et al., 1993; Copenhaver et al., 1993; Smith, 1970; etc.).

Various studies concerning the three-dimensional aspects of endwall flows in axial compressors have been reported. Dring et al. (1982, 1983) investigated the flow in an isolated rotor with high aerodynamic loading and low aspect ratio. The observed regions of high loss were near the end walls. At the hub, the high loss was associated with the flow separation of the blade and endwall surface boundary layers near the trailing edge of

the suction surface. At the tip, the high loss region was thought to be due to the rotor tip leakage flow. When the flow coefficient was reduced, the high loss region near the hub extended radially over the entire span. On the rotors of a two-stage machine (Dring et al., 1983), large areas of separated flow on the surfaces near the hub were identified through flow visualization. Joslyn and Dring (1985) performed a similar study of the flow field in a second-stage stator. A stalled region with high aerodynamic loss in the corner of the suction surface and the hub end wall was reported in their study. This corner stall extended up to 75 percent span at a reduced flow rate. They found that the flow incidence angle at the stator hub leading edge was increased due to the rotor hub corner stall, which caused severe flow separation on the stator suction surface near the hub end wall. Dong et al. (1987) investigated flow and loss mechanisms in a single-stage low-speed axial flow compressor. They did not find endwall flow separation in the rotor. However, large separated areas were observed at both endwalls of the stator. Schulz and Gallus (1988) performed detailed flow measurements in an isolated subsonic compressor stator at various blade loadings. Their extensive measurements included blade and endwall flow visualization, steady and unsteady static pressure measurements, blade boundary layer investigations with hot wires and hot films, and five-hole probe measurements at the stator exit. In their study, hub corner stall was observed at all blade loadings. The hub corner stall and the related secondary flows were responsible for the high loss region observed at the stator exit.

Certain high-speed fan/compressor designs use the concept of high-performance hub design to prevent possible hub corner stall and its related performance deterioration. During the 1994 ASME/IGTI CFD code assessment exercise, a large dip in the measured spanwise distribution of total pressure was observed near the hub for the case under study. Because the measurements

Contributed by the International Gas Turbine Institute and presented at the 42nd International Gas Turbine and Aeroengine Congress and Exhibition, Orlando, Florida, June 2–5, 1997. Manuscript received International Gas Turbine Institute February 1997. Paper No. 97-GT-42. Associate Technical Editor: H. A. Kidd.

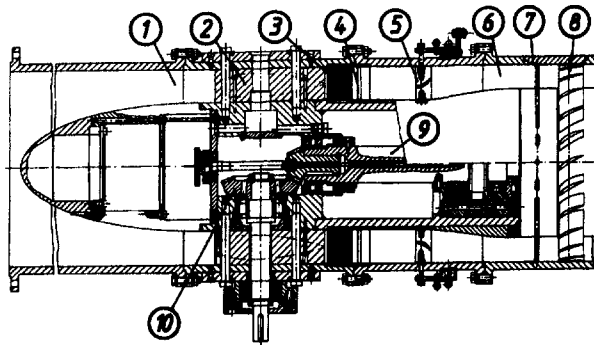


Fig. 1 Annular cascade test facility

did not include flow visualization or LDV data near the hub, no direct explanation could be made. This total pressure deficiency near the hub, however, disappeared at the reduced blade loading, which occurred at 60 percent rotor speed. Hub corner stall was considered to be one of the possible causes of the observed total pressure deficiency near the hub at 100 percent rotor speed at near-peak efficiency.

The primary objective of the current study is to advance our understanding of the basic mechanism of compressor hub corner stall. Both experimental data and numerical results are analyzed in detail for the flows in a subsonic compressor stator and in a transonic compressor rotor.

### Hub Corner Stall in a Subsonic Compressor Stator

A detailed experimental study to investigate hub corner stall was conducted by Schulz and Gallus (1988). The test facility is shown in Fig. 1. The extensive and comprehensive data base includes the following measurements:

- 1 Visualization of the flow on the blades, hub, and casing (dye injection and oil flow technique)
- 2 Wall static pressure measurements
- 3 Steady and unsteady blade pressure measurements
- 4 Blade boundary layer investigations with hot-wire and hot-film probes
- 5 Five-hole probe measurements at the stator exit

A turbocompressor set provides continuous airflow to the test rig. The swirl angle of the flow can be varied by means of 48

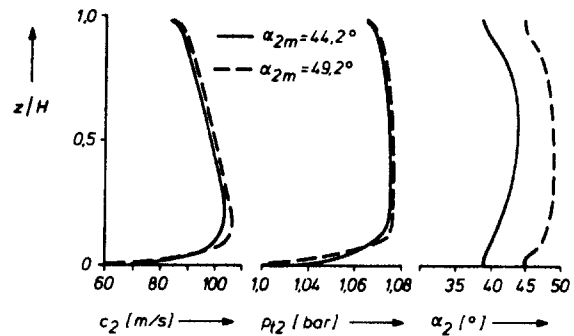


Fig. 3 Flow properties at cascade inlet

adjustable inlet guide vanes (⑤ in Fig. 1). The test compressor cascade (⑧ in Fig. 1) consists of 24 untwisted blades mounted on the hub, with a hub-to-tip ratio of 0.75 and a tip diameter of 428 mm. The aspect ratio is 0.86 and the solidity at midspan is 0.78. The blade profiles are radially stacked at their center of gravity and the blade metal angles at inlet and exit are 44 and 15 deg respectively. Other geometric parameters are shown in Fig. 2.

For the investigation described in this paper, the experiment was performed with the rotor removed during the test. The properties of the incoming flow were surveyed with pneumatic five-hole and boundary layer probes at 56 percent blade chord upstream of the stator leading edge. Inlet flow conditions were specified at the same location for the calculation as well. The inlet angle to the stator, and therefore the blade loading, were varied, and the measurements were taken at five different points of operation identified by the inlet angles at midspan. The data were taken at inlet angles of 40, 44.2, 49.2, 54.6, and 57.6 deg. These angles are measured from the axial direction, and zero-incidence occurs at an inlet angle of 42 deg. The spanwise distributions of inlet velocity, total pressure, and inlet angle for the midspan inlet angles of 44.2 and 49.2 deg are shown in Fig. 3. The instrumentation and the accuracy of the measurements are described in more detail by Schulz and Gallus (1988) and Gallus et al. (1991).

The steady Reynolds-averaged Navier-Stokes equations are solved for the current problem. For the present numerical study, the entire flow field is assumed to be turbulent and no transition is considered. To close the system of equations, a closure model for turbulence stresses must be applied. Although no existing closure model accurately represents all salient flow features, the main flow phenomena in turbomachinery can be adequately calculated by the current generation of turbulence models. For

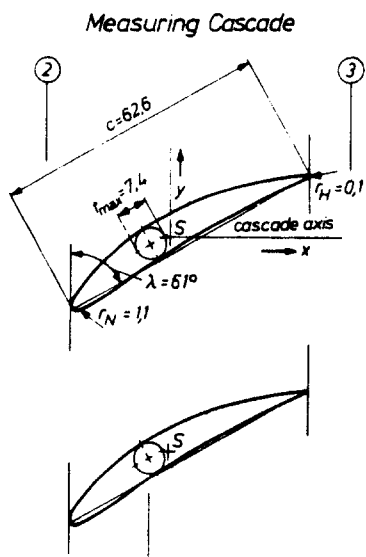


Fig. 2 Midspan cascade geometry

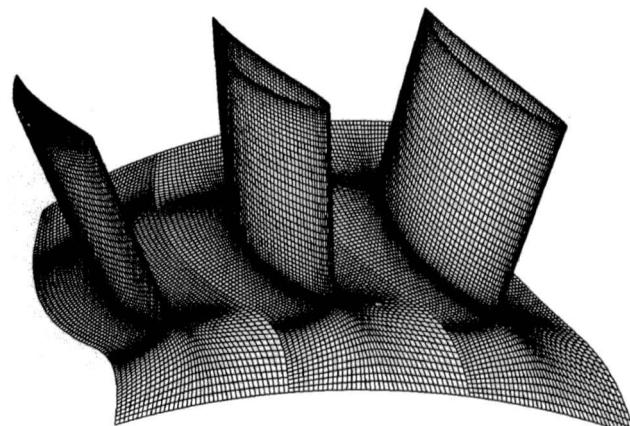
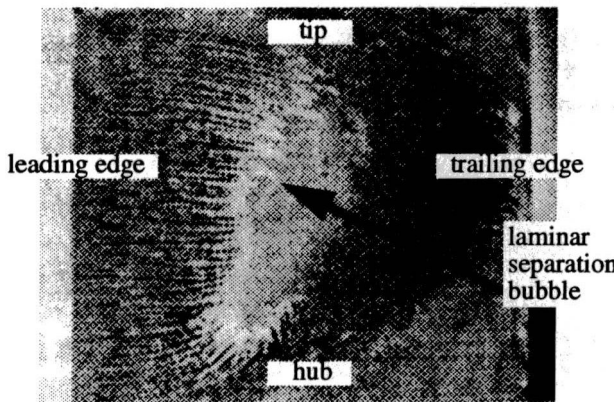
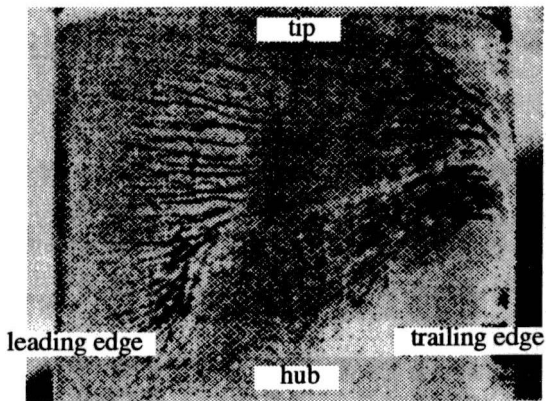


Fig. 4 Computational grid for compressor stator



5a) 44.2 degree inlet flow angle



5b) 49.2 degree inlet flow angle

Fig. 5 Oil flow visualization on blade suction surface

the current numerical study, a standard two-equation turbulence model with a low-Reynolds-number modification is applied. Standard values for the various coefficients in the turbulence model are used for the current hub corner stall study. The details of the applied turbulence model are given by Hah and Wennerstrom (1991). The governing steady Reynolds-averaged Navier-Stokes equations are solved with a pressure-based implicit relaxation method using a fully conservative control volume approach described by Hah (1987).

At the inflow boundary, the measured distributions of total pressure, total temperature, and inlet flow angle are fixed. At the outflow boundary, the static pressure is fixed at the shroud and all the other flow variables are extrapolated. The experimental value of the turbulence kinetic energy is prescribed at the inflow boundary and a standard equilibrium condition is used to estimate the length scale for the turbulence dissipation. Periodicity conditions are applied between individual blades. Residuals of each finite difference equation are integrated over the entire domain. When the total integrated residuals of all the equations are reduced by four orders of magnitude from the initial values, the solution is considered to be converged. The computational grid, shown in Fig. 4, has 50 nodes in the blade-to-blade direction, 47 nodes in the spanwise direction, and 102 nodes in the streamwise direction. Typical computing time is about one hour on a Cray-YMP.

**Flow Field Near Blade Suction Surface and Hub Wall.** Experimental flow visualizations, created by dye injection, on the blade suction surface at inlet flow angles of 44.2 and 49.2 deg are shown in Fig. 5. At both blade loadings, the reversed flow region near the hub is larger than that near the tip. This is

because the incoming hub boundary layer is thicker than that at the shroud, as shown in Fig. 3. A hub surface flow visualization at an inlet flow angle of 44.2 deg is shown in Fig. 6. This hub flow visualization indicates that there are two distinct vortices on the hub wall. Calculated flows near the suction surface and on the hub wall are shown in Fig. 7 in the form of surface particle traces and velocity vectors. The numerical solutions also show that the reversed flow region near the hub is larger than that near the shroud. The stalled flow region also increases with higher blade loading. The numerical results agree very well with the measurements.

The flow visualizations and numerical results indicate that two distinct vortices exist near the hub surface. The larger vortex is centered away from the suction surface at approximately 80 percent axial chord downstream from the leading edge. The smaller vortex is located very close to the trailing edge. The two vortices are clearly seen at both blade loadings in the calculated results. The hub surface flow visualization supports the calculated results. The blade suction surface flow visualization shown in Fig. 5 indicates that there exists a laminar flow separation bubble near the middle of the blade span. This laminar separation bubble was also confirmed through hot-film measurements (Schulz and Gallus, 1988). Inside the separation bubble, the flow undergoes transition and reattaches as turbulent flow. In the computations, the flow is assumed to be completely turbulent. This assumption might contribute to the deviation between the measurements and the calculations. However, the measured incoming flow near the hub is turbulent and the flows near the end walls seem to remain turbulent. Therefore, the current fully turbulent flow calculations appear to be adequate for the hub corner stall investigation.

**Topological Structure of Hub Corner Stall.** Comparisons between the surface flows from the measurements and the calculation indicate that the numerical solution represents the hub corner stall reasonably well. Therefore, an attempt was made to use the numerical solution to shed some new light on the complex structure of the hub corner stall. Although surface flow visualization is very helpful in understanding flow near solid walls, surface flow patterns do not necessarily explain complex flow patterns away from the walls. For the current problem, experimental flow visualization is not possible away from the wall surfaces because of high flow velocity. Probe measurements exhibit large errors and disturb the flow itself beyond tolerable limits, and laser velocimetry for this type of three-dimensional separated flow near the endwall has not been practical due to seeding problems. Numerical solutions, however,

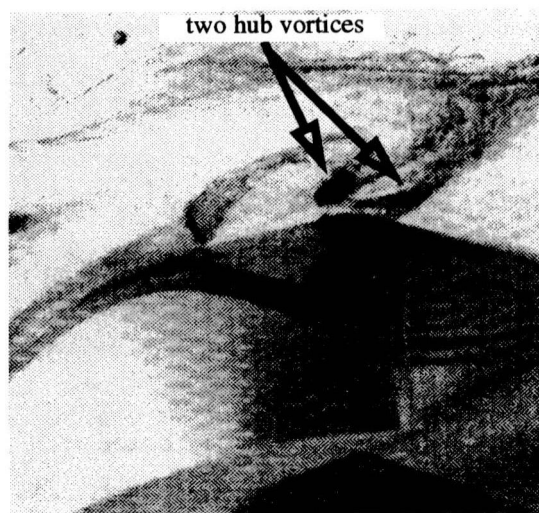
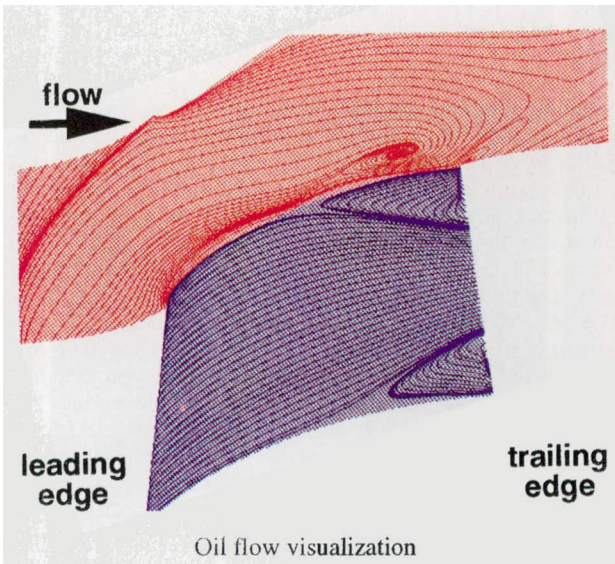
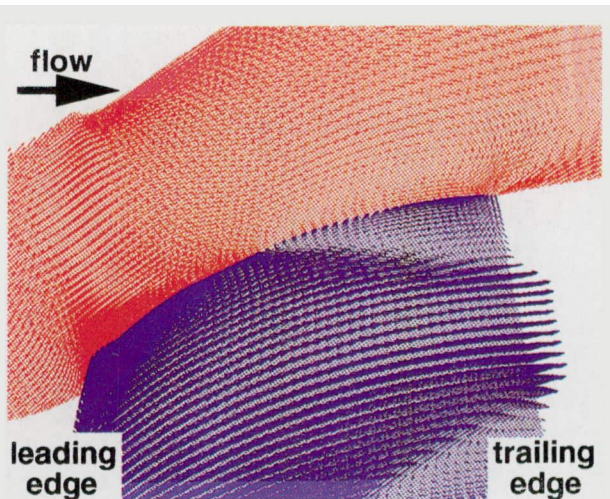


Fig. 6 Oil flow visualization on hub surface

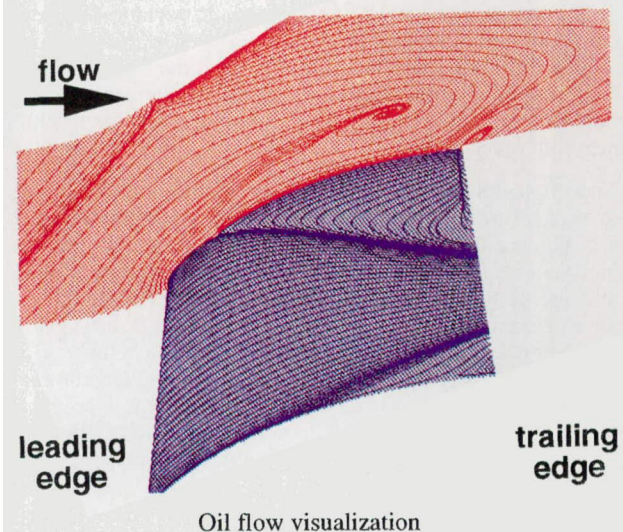


## Oil flow visualization

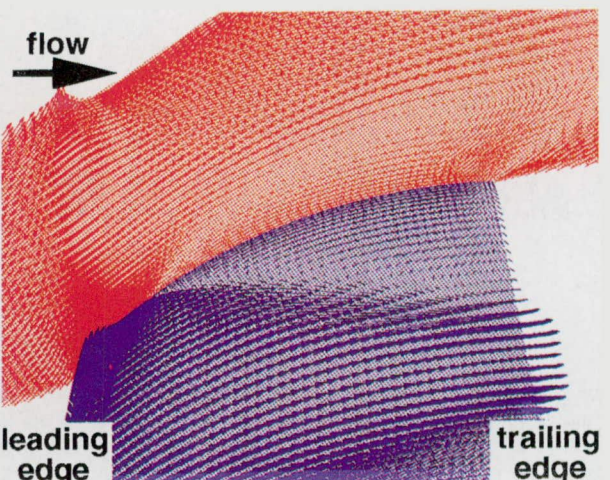


## Velocity vectors near surface

Fig. 7(a) Calculated flow near hub and suction surface (44.2 deg inlet flow angle)



## Oil flow visualization



## Velocity vectors near surface

Fig. 7(b) Calculated flow near hub and suction surface (49.2 deg inlet flow angle)

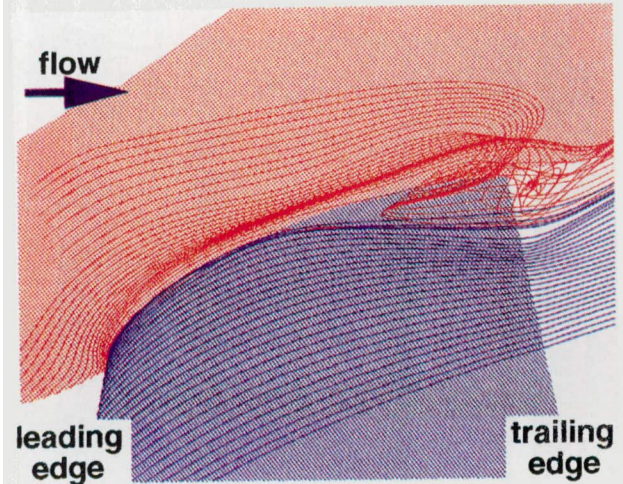


Fig. 8 Particle traces in vortex (44.2 deg inlet flow angle)

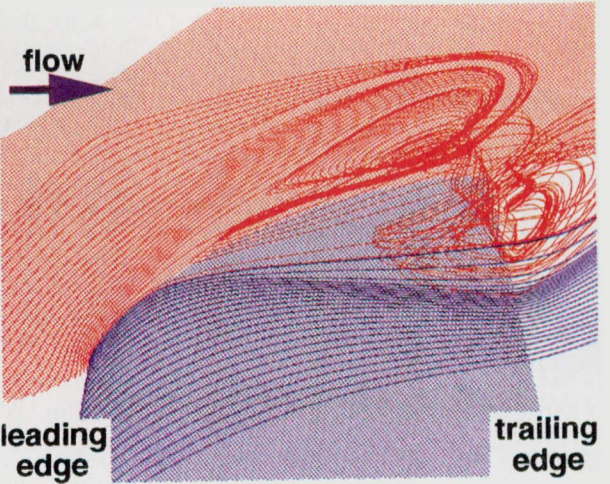


Fig. 9 Particle traces in vortex (49.2 deg inlet flow angle)

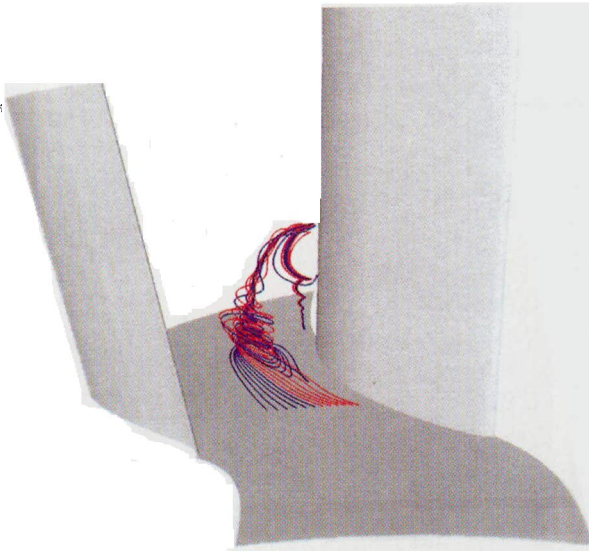


Fig. 10 Structure of hub corner stall vortex

compliment the experimental data by filling in the gaps where measurements cannot be made.

According to Fig. 7, two distinct vortices are clearly shown on the hub wall. On the other hand, no clear vortex structure can be identified on the suction surface, although a reversed flow region is clearly visible near the corner. The flow structures visualized on the hub wall and the suction surface must be part of a three-dimensional structure of hub corner stall. To visualize this three-dimensional structure, particle traces were generated from the numerical solution. Figures 8 and 9 show particle traces inside the hub corner stall at two blade loadings. The structures of the hub corner stall are very similar at the different loadings, but the details of the flow structure are clearer at the higher blade loading. The structure of the vortex itself is shown in Fig. 10. The dominant features of the hub corner stall appear to be two vortices. One is located near the suction surface at approximately 80 percent axial chord, and the other is located close to the trailing edge. These two counterrotating vortices extend radially outward and connect outside the wall boundary layer. Thus, the vortices visualized on the hub wall are actually

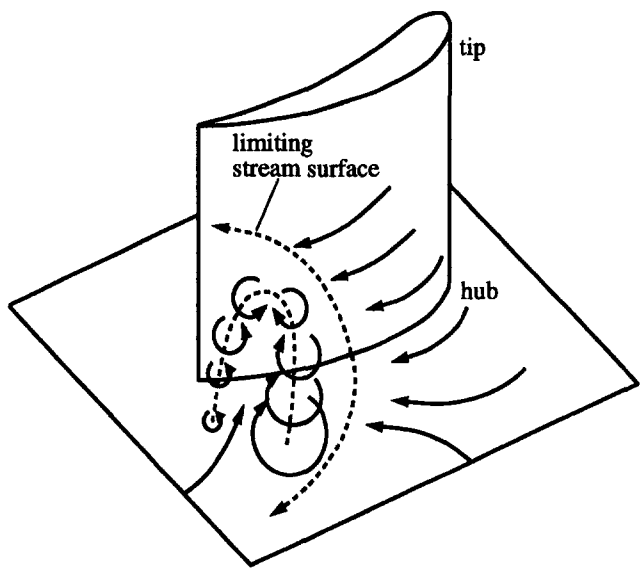


Fig. 11 Topology of hub corner stall

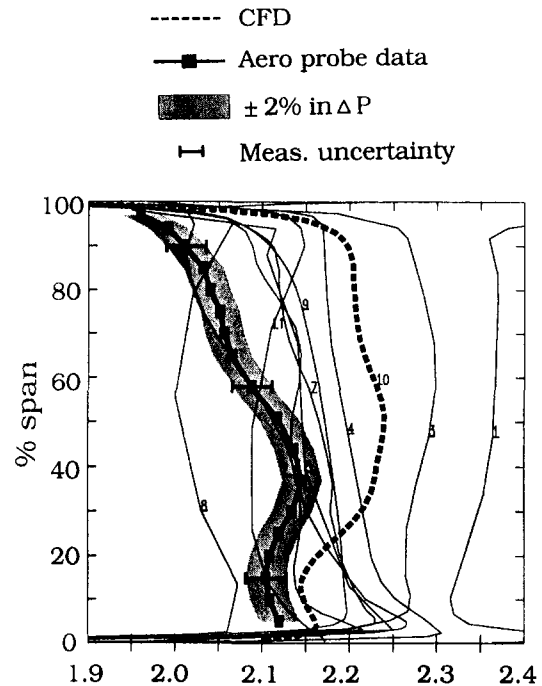


Fig. 12 Radial total pressure distributions for Rotor 37

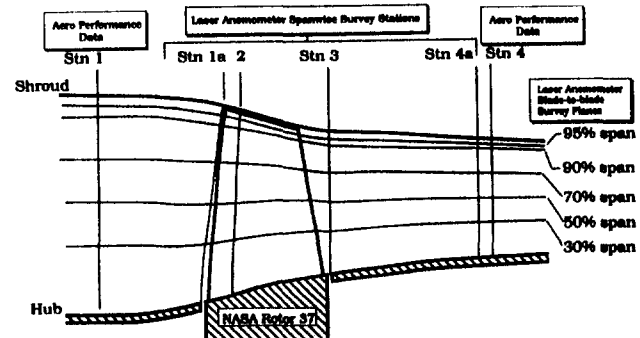
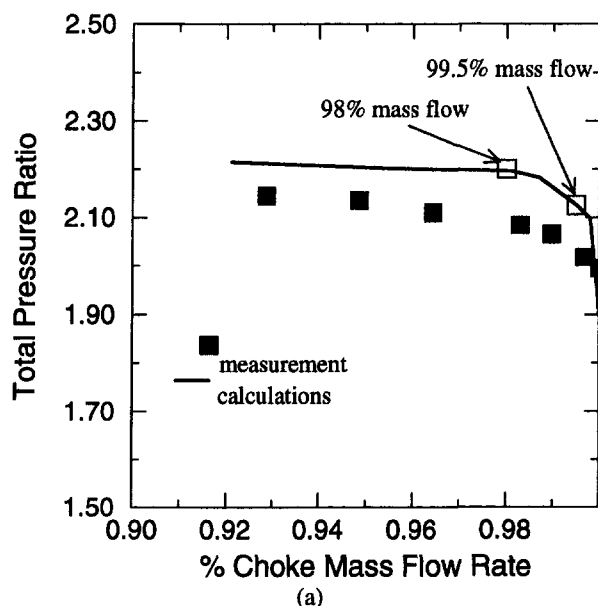


Fig. 13 Experimental measurement stations for Rotor 37

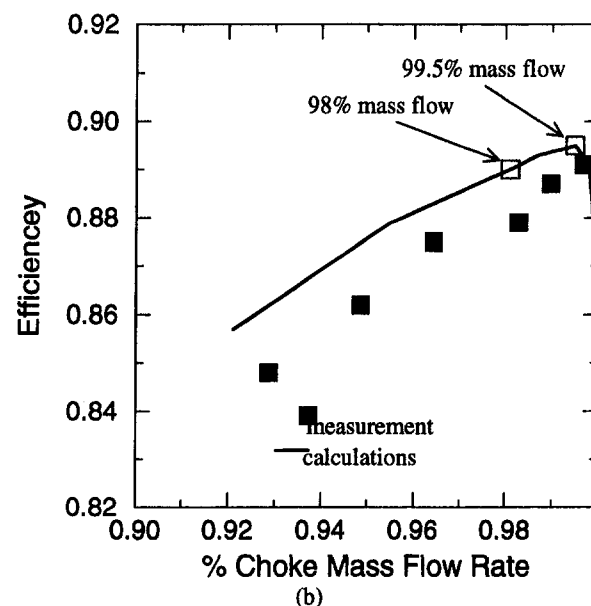


Fig. 14 Computational grid for Rotor 37

two legs of a single vortex. Because of the strong particle motion around this vortex, a reversed flow region and a limiting streamline are created on the suction surface. The structure of the hub corner stall is also illustrated in Fig. 11. The single vortex, whose two legs originate from the hub, clearly explains the measured flow pattern on the hub and the blade suction surface. Again, the dominant feature of the hub corner stall in a compres-



(a)



(b)

Fig. 15 Comparison of rotor performance for Rotor 37

sor stator is a twisterlike vortex that has two legs attached on the hub wall. The location and the strength of this vortex depend on the blade loading (or diffusion factor) and the incoming flow characteristics, among other factors. The tested airfoils operate below the conventionally accepted limit of the diffusion factor. Therefore, a simple diffusion factor cannot be used as a criterion for the occurrence of compressor hub corner stall. Design optimization to remove or control this hub corner stall vortex with currently available numerical tools might improve the performance of multistage compressors.

#### Hub Corner Flow in a Transonic Compressor Rotor

During the 1994 ASME/IGTI Turbo Expo, a CFD code assessment exercise was organized by the Turbomachinery technical committee. The objective of this exercise was to provide an objective view of CFD capabilities to the turbomachinery aerodynamics community. Both CFD users and CFD developers were invited to submit solutions for a "blind test case" to the

organizers. The flow in a transonic axial compressor, designated as Rotor 37, was used for the test. Eleven blind computations were submitted. Comparisons between the calculations and the measurements were presented during the 1994 IGTI Conference (Strazisar and Denton, 1995). The experimental results were reported by Suder and Celestina (1996) and Suder (1996). The flow field was also used extensively as a test case in CFD validation for propulsion system components (Dunham, 1998).

As is widely recognized in the turbomachinery aerodynamics CFD community, the current generation of CFD codes provides very useful numerical solutions for design purposes. The most useful information from CFD solutions is obtained by calculating variations between different designs. Because current turbulence models do not accurately represent the complexity of real flows, and numerical procedures need further refinements, CFD calculations do not always predict absolute values of aerodynamic properties accurately. However, accurate prediction of changes in aerodynamic parameters due to changes in the design can be more important than the prediction of absolute values.

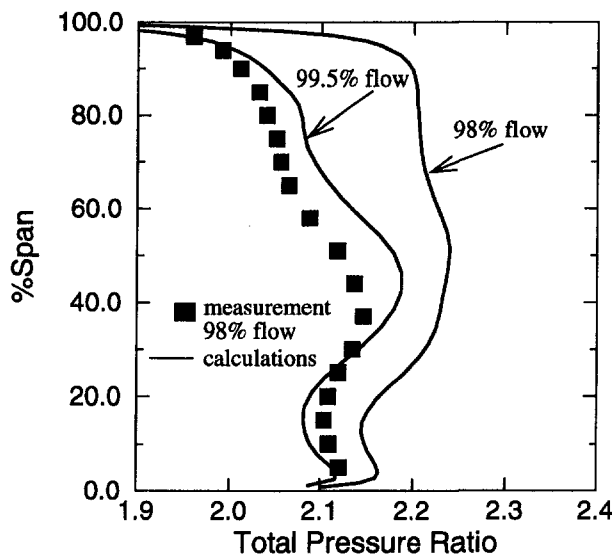


Fig. 16 Comparison of total pressure distribution

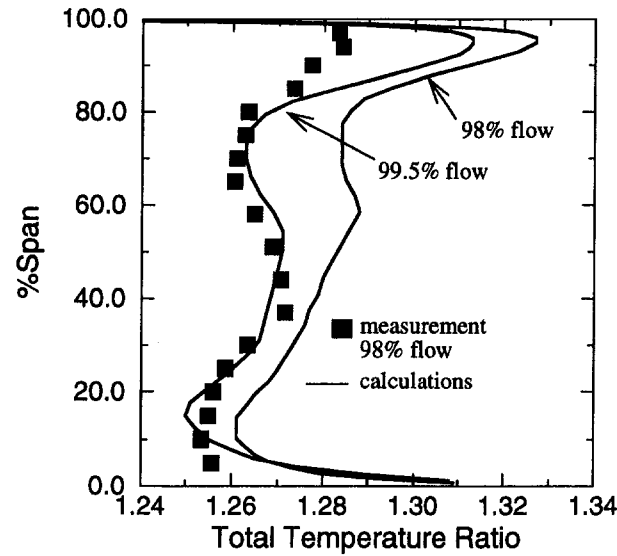


Fig. 17 Comparison of total temperature distribution

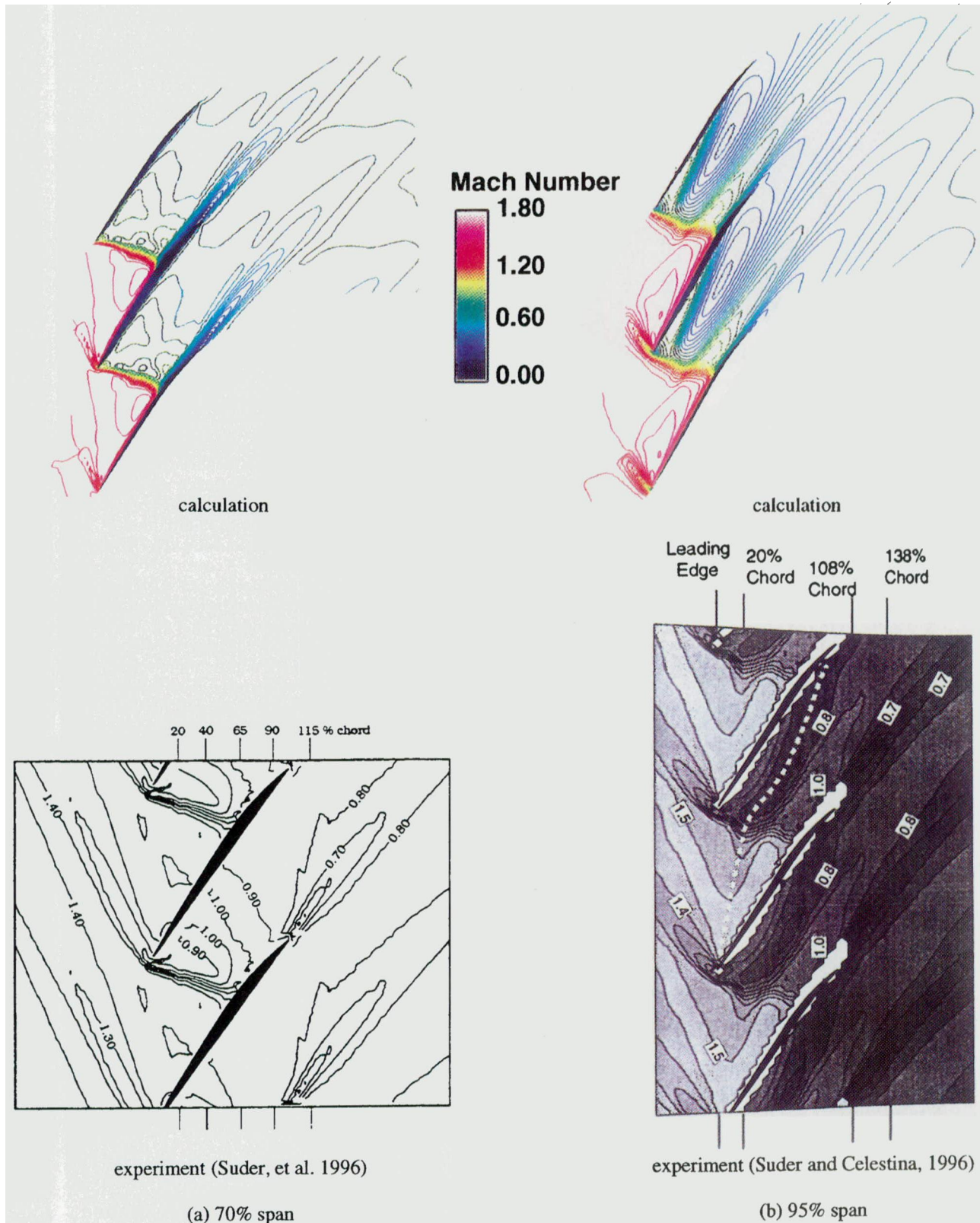


Fig. 18 Calculated and experimental relative Mach number distributions for Rotor 37

Accurate prediction of the shapes of spanwise property distributions can also be more useful than absolute values of integrated properties. Although the numerical results for the blind test case showed wide variations, the various numerical solutions revealed many interesting flow features and the exercise was

very helpful in understanding the current level of the technology.

One of the observations during the exercise was that the spanwise shape of the total pressure distribution was not predicted very well, as shown in Fig. 12. Some solutions matched

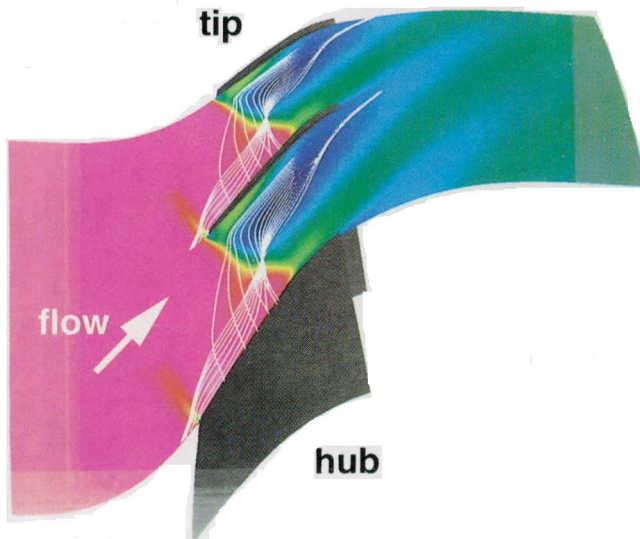


Fig. 19 Tip clearance vortex and passage shock interaction

the overall integrated level well without matching the shape at all. The measurement shows a large dip in the total pressure distribution near the hub. The measured shape of the total pressure distribution near the hub was predicted by solution 10, which was submitted by the authors. However, solution 10 overpredicted the total pressure rise significantly in the outer half-span. During the workshop, it was pointed out that solution 10 shows a mild hub corner stall at the specified operating condition, and this was proposed as the reason for the dip in the spanwise profile of total pressure near the hub.

In this section, the calculated flow fields of Rotor 37 at different flow conditions are further analyzed and compared with the available data. The objective of the analysis is to investigate whether hub corner stall occurs at the given flow conditions and to compare the flow structures with those observed in the subsonic compressor stator. The analysis is based on the numerical solutions submitted during the blind test exercise. No new calculations were performed to better match the measurements in terms of absolute values.

The flow field was calculated with the same CFD code that was used to calculate the flow in the subsonic compressor stator reported in the previous section. The applied turbulence model is also the same. The measurement stations and the computational grid are shown in Figs. 13 and 14. The grid consists of 58 nodes in the blade-to-blade direction, 51 nodes in the spanwise direction, and 151 nodes in the streamwise direction. To describe the blade tip geometry, ten computational nodes are distributed tangentially across the blade tip and 10 nodes are located radially between the blade tip and the shroud. After the blind test exercise, the computational grid was refined to  $114 \times 91 \times 181$ . However, changes in the calculated solutions due to the grid refinement were not significant.

The measured and the calculated rotor speed lines are shown in Fig. 15 in the form of the total pressure ratio and the adiabatic efficiency. Previous code validation experiences have indicated that the code predicts slightly optimistic performance relative to that indicated by measurements. The deviation shown in Fig. 15, especially in terms of the total pressure ratio, is significantly larger than normally observed. Some possible causes of the deviation will be discussed later in this section.

Various aerodynamic measurements were made near the peak efficiency condition. Although the measured peak efficiency occurs very close to the choke condition (between 99 and 99.5 percent of the choke mass flow rate) according to the data shown in Fig. 15, the comparisons were made at 98 percent of the choke mass flow rate. Calculated spanwise distributions of

total pressure at measurement station 4 are compared with the measurements in Fig. 16. Calculated values at 99.5 percent of the choke mass flow rate are also presented in Fig. 16. The solution at 98 percent of choke mass flow rate, which was presented during the original exercise, shows a much higher pressure rise near shroud than the measurement. This observation suggests that another comparison at lower back pressure might show better agreement with the measurements. A comparison of total temperature distributions at station 4 is given in Fig. 17. The comparisons in Figs. 16 and 17 indicate that relatively small shifts in the operating condition produce quite different absolute values of total pressure and total temperature. It is very interesting to observe that the numerical results at 99.5 percent of choke mass flow rate agree much better with the measurements than those at 98 percent of the choke mass flow rate. As shown in Fig. 16, the calculated spanwise distributions of total pressure at both flow conditions show a dip near the hub like the experimental data.

Figure 18 compares relative Mach number distributions between the measurements and the calculation at 70 and 95 percent span. The results indicate that the calculated flow field agrees well with the measured flow field in terms of location and strength of the passage shock structure. As shown in Fig. 18, a low Mach number region is formed after the passage shock near the pressure surface at 95 percent span. Figure 19 shows particle traces generated from the numerical solution to identify the origin of this region, which is considered to have a strong link to the onset of compressor stall. According to the particle traces shown in Fig. 19, the tip clearance vortex, which initiates near the leading edge, interacts with the passage shock, and the interaction seems to contribute to the formation of this low momentum area. Because of this interaction, the front of the passage shock moves forward at the interaction location. This forward movement of the passage shock is more clearly seen at 98 percent span, as shown in Fig. 20.

**Flow Structure Near Hub and Blade Suction Surface Corner.** Velocity vectors and particle traces near the hub and the suction side of the blade are shown in Fig. 21 at 98 percent of the choke flow rate. Figure 22 shows velocity vectors and corresponding particle traces at 99.5 percent of the choke mass flow rate. Very similar structures are observed at the two mass flow rates. A weak hub corner stall is observed in Fig. 22. Three-dimensional particle traces were generated to identify any existing vortex structure and the results are shown in Fig. 23. A weak vortex structure is identified. Compared to the hub corner stall vortex observed in the compressor stator, this vortex has only one leg on the hub wall and the other end of the vortex is diffused in the free stream before touching the hub wall again. Less pronounced hub corner stall in the rotor compared to that

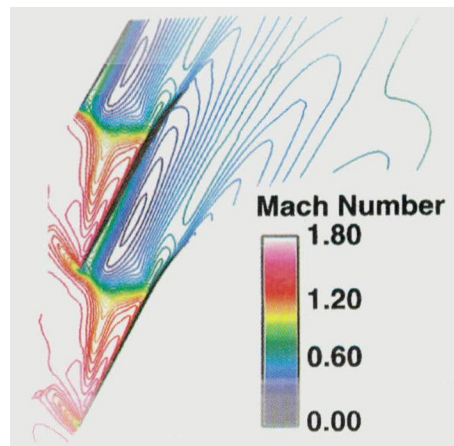


Fig. 20 Relative Mach number distribution at 98 percent span

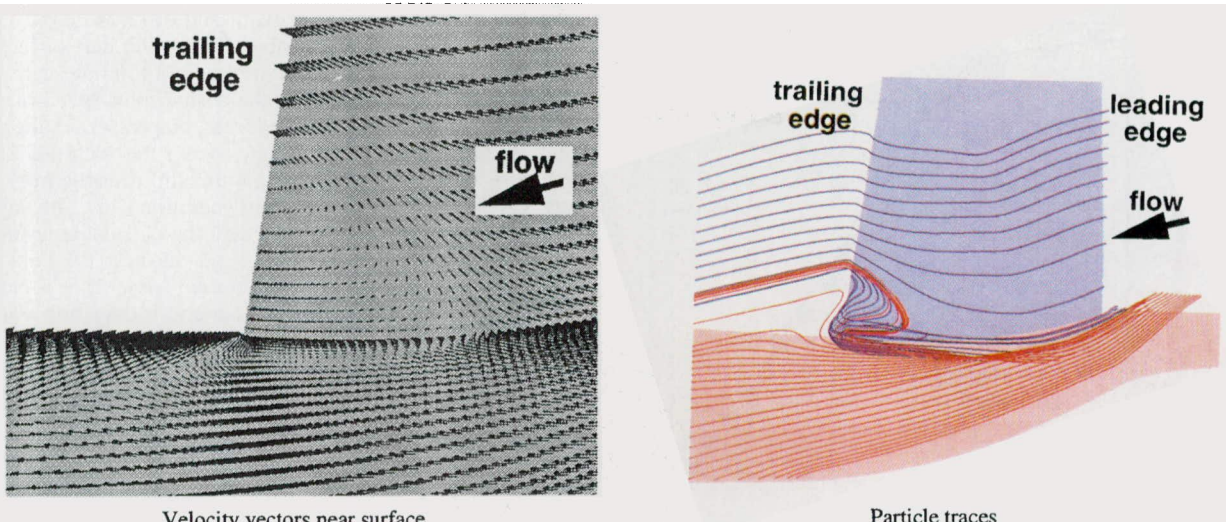


Fig. 21 Calculated flow near hub at 98 percent choke mass flow rate

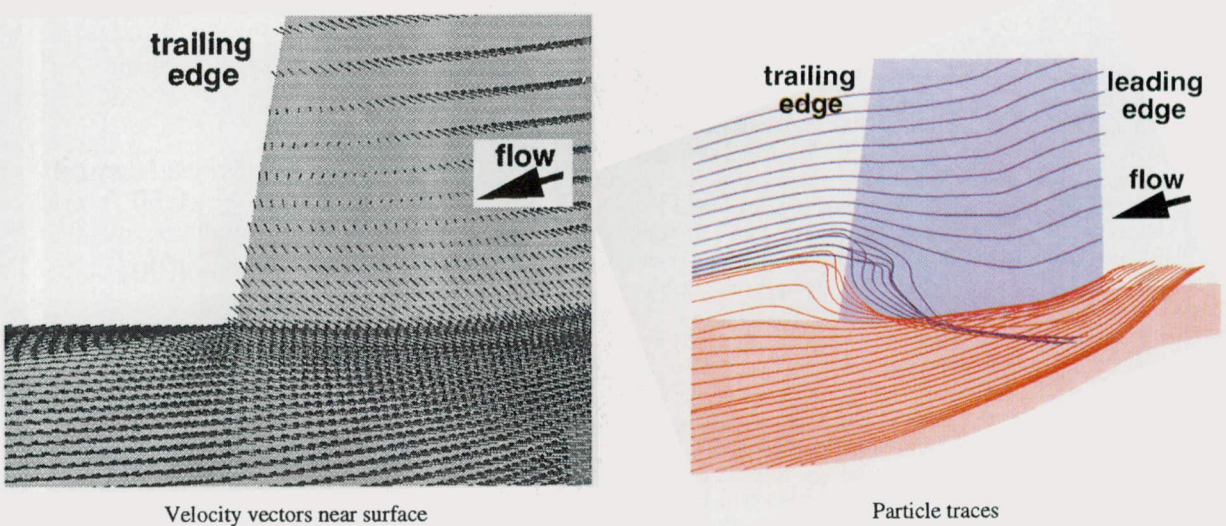


Fig. 22 Calculated flow near hub at 99.5 percent choke mass flow rate

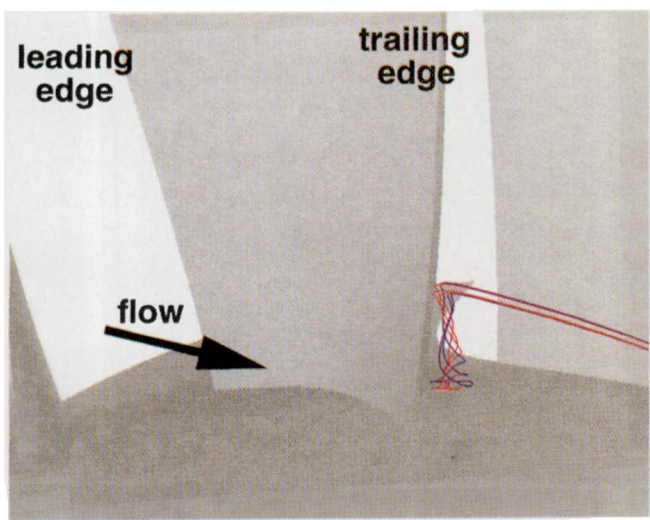


Fig. 23 Particle traces for hub corner flow at 98 percent choke mass flow rate

in the stator has been reported by Dring et al. (1982) and Dong et al. (1987).

Further aerodynamic performance measurements (Suder et al., 1996) show that the dip in the total pressure distribution shown in Fig. 12 disappears at the reduced blade loading that occurs at 60 percent rotor speed. In Fig. 24, the spanwise distribution of total pressure ratio at this operating condition is compared between the measurements and the calculation. Calculated and measured relative Mach number distributions at 95 percent span at this operating condition are compared in Fig. 25. Again the calculated flow field represents the measured flow field very well. Calculated velocity vectors and particle traces at this operating condition are given in Fig. 26. The results in Figs. 24 and 26 indicate that the hub corner stall does not occur at this reduced blade loading. The results shown in Figs. 16–26 suggest that the dip in the radial total pressure distribution near the design rotor speed is due to compressor hub corner stall. The possibility of any direct experimental verification of the existence of hub corner stall in Rotor 37 is very remote at the moment. Because of the twisted blade shape, access of a laser beam to the hub location from an optical window located on the shroud is almost impossible. The rotor speed also prohibits any useful flow visualization near the hub.

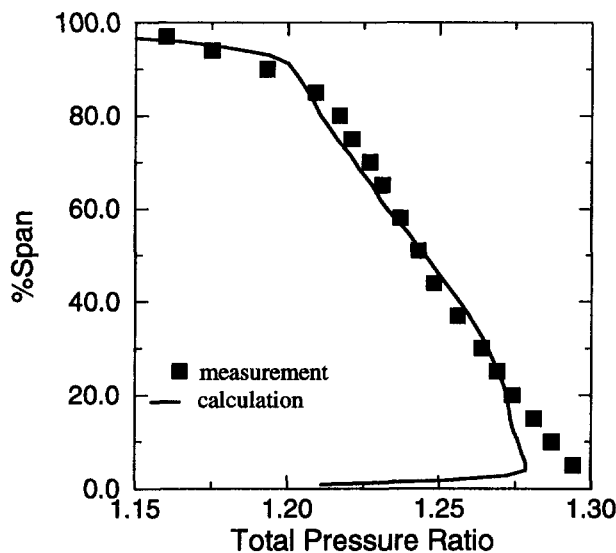


Fig. 24 Comparison of spanwise total pressure distribution near peak efficiency at 60 percent rotor speed

Some of the disagreements between the calculation and the measurements can be attributed to the following facts. For the numerical analysis, it is assumed that all 36 rotor passages are identical, with a uniform clearance gap. The measurements, however, show considerable variations in measured flow variables between blade passages. As shown in Fig. 13, there is a small gap between the stationary part of the hub and the rotating part of the hub, and there might be a small leakage flow from this gap. As is widely known, the flow field in a transonic compressor rotor is extremely sensitive to small changes in the geometry or flow condition. All of these differences between the numerical set up and the experimental conditions may contribute to differences in the effective blockage in the passage, which could explain why the values calculated at the slightly higher mass flow rate match the measured values better.

At both operating conditions at the design rotor speed, the numerical solutions show a mild hub corner stall, which corresponds to the observed dip in the total pressure distribution. At the reduced rotor speed, the measurements do not show this dip in the radial distribution of total pressure. The numerical solution predicts neither hub corner stall nor a dip in the total pressure near the hub, in agreement with the measurements. Therefore, the observed dip in total pressure rise near the hub at the design rotor speed may be caused by hub corner stall. Another possible cause may be leakage into the main stream from the small gap just upstream of the rotor at the hub, as investigated by Shabbir et al. (1997).

### Concluding Remarks

This study was performed to advance our understanding of compressor hub corner stall. Three-dimensional flow fields in a subsonic compressor stator and in a transonic compressor rotor were used for the study. Numerical solutions based on the Reynolds-averaged Navier-Stokes equations and available experimental data were analyzed to construct detailed flow structures of compressor hub corner stall. The current study reveals that a vortex is formed at the corner of the hub and the blade suction surface toward the rear of the blade passage. The strong twisterlike vortical motion causes reversed flow regions on the hub surface as well as on the blade suction surface. In the compressor stator, the end of the vortex turns back to the hub surface. According to the numerical results, the two counterrotating vortices that have been identified through oil flow visualization are actually two legs of a single vortex. In the

rotor, this vortex bends downstream and diffuses quickly, and only one leg of the vortex is observed on the hub surface. A measured dip in the spanwise distribution of total pressure near the hub of the transonic rotor at the design rotor speed may be due to hub corner stall. At the reduced compressor loading that occurs at 60 percent rotor design speed, the measured total pressure distribution does not show this dip near the hub. The numerical solution at this operating condition shows no sign of hub corner stall in particle traces, and the calculated spanwise distribution of total pressure shows no dip near the hub. The present study reveals that compressor hub corner stall is caused by a three-dimensional vortex system and it does not seem to be correlated with a simple diffusion factor. Design concepts for high-performance stages can possibly be developed to remove or control hub corner stall using currently available nu-

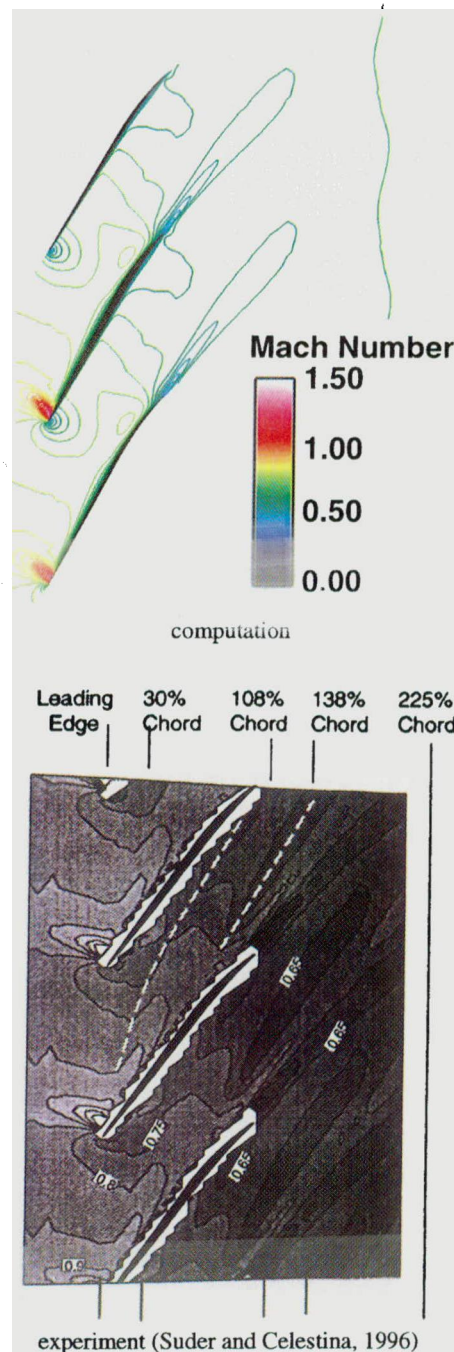


Fig. 25 Comparison of relative Mach number at 95 percent span and 60 percent rotor speed

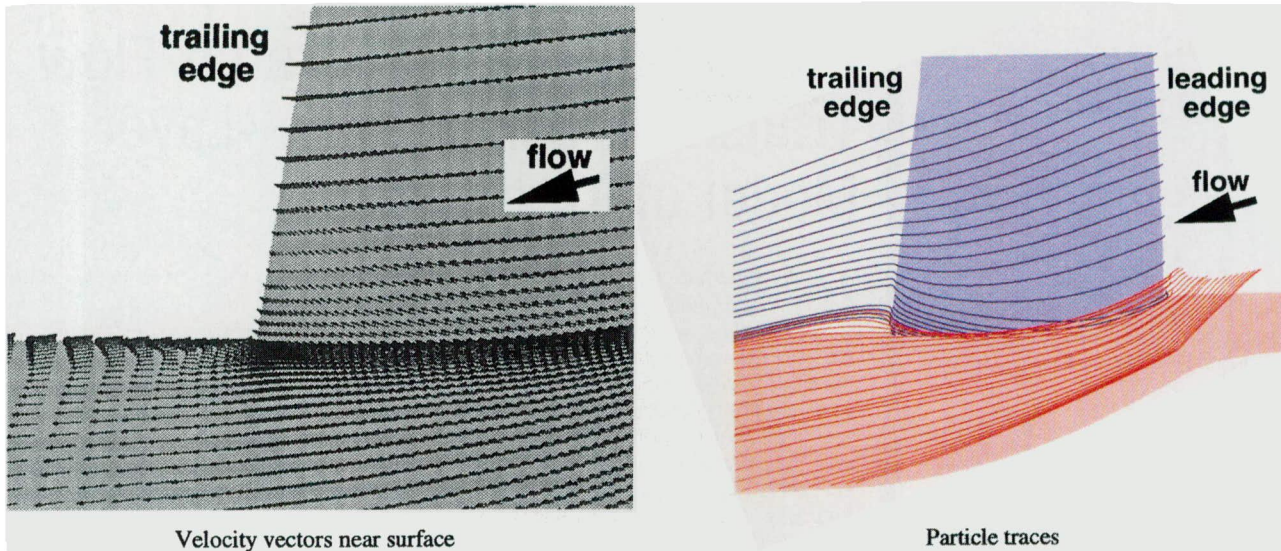


Fig. 26 Calculated flow near hub at 60 percent rotor speed

merical techniques. More detailed experimental data bases for hub corner stall, especially in compressor rotors, will be very useful in calibrating numerical tools as well as in developing such concepts.

### Acknowledgments

The authors would like to acknowledge the contribution of F. Tsung of ICOMP at NASA Lewis Research Center in preparing the illustrations. Also, we would like to thank Dr. A. J. Strazisar and Dr. K. L. Suder of NASA Lewis Research Center for many valuable discussions about the experimental data.

### References

- Damczyk, J. J., Celestina, M. L., and Greitzer, E. M., 1993, "The Role of Tip Clearance in High-Speed Fan Stall," *ASME JOURNAL OF TURBOMACHINERY*, Vol. 115, No. 1, pp. 28–39.
- Copenhafer, W. W., Hah, C., and Puterbaugh, S. L., 1993, "Three-Dimensional Flow Phenomena in a Transonic, High-Throughflow Compressor Stage," *ASME JOURNAL OF TURBOMACHINERY*, Vol. 115, pp. 240–248.
- Dong, Y., Gallimore, S. J., and Hodson, H. P., 1987, "Three-Dimensional Flows and Loss Reduction in Axial Compressors," *ASME JOURNAL OF TURBOMACHINERY*, Vol. 109, pp. 354–361.
- Dring, R. P., Joslyn, H. D., and Hardin, L. W., 1982, "An Investigation of Compressor Rotor Aerodynamics," *ASME Journal of Engineering for Power*, Vol. 104, pp. 84–96.
- Dring, R. P., Joslyn, H. D., and Wagner, J. H., 1983, "Compressor Rotor Aerodynamics," AGARD-CP-351, Copenhagen.
- Dunham, J., 1998, "CFD Validation for Propulsion System Components," AGARD Advisory Report 355.
- Gallus, H. E., Hah, C., and Schulz, H. D., 1991, "Experimental and Numerical Investigation of Three-Dimensional Viscous Flows and Vortex Motion Inside an Annular Compressor Blade Row," *ASME JOURNAL OF TURBOMACHINERY*, Vol. 113, No. 1, pp. 198–206.
- Hah, C., 1987, "Calculation of Three-Dimensional Viscous Flows in Turbomachinery With an Implicit Relaxation Method," *AIAA Journal of Propulsion and Power*, Vol. 3, No. 5, pp. 415–42.
- Hah, C., and Wennerstrom, A. J., 1991, "Three-Dimensional Flowfields Inside a Transonic Compressor With Swept Blades," *ASME JOURNAL OF TURBOMACHINERY*, Vol. 113, No. 1, pp. 241–251.
- Joslyn, H. D., and Dring R. P., 1985, "Axial Compressor Stator Aerodynamics," *ASME Journal of Engineering for Gas Turbines and Power*, Vol. 107, pp. 485–493.
- Schulz, H. D., and Gallus, H. D., 1988, "Experimental Investigations of the Three-Dimensional Flows in an Annular Compressor Cascade," *ASME JOURNAL OF TURBOMACHINERY*, Vol. 110, pp. 467–478.
- Shabbir, A., Celestina, M. L., Adamczyk, J. J., and Strazisar, A. J., 1997, "The Effect of Hub Leakage Flow on Two High Speed Axial Flow Compressor Rotors," *ASME Paper 97-GT-346*, to be published in the *ASME JOURNAL OF TURBOMACHINERY*.
- Smith, L. H., Jr., 1970, "Casing Boundary Layers in Multistage Axial Flow Compressors," in: *Flow Research on Blading*, L. S. Dzung, ed., Elsevier Publishing Company, Amsterdam, No. 3, pp. 688–690.
- Strazisar, A. J., and Denton, J. D., 1995, "CFD Code Assessment in Turbomachinery—A Progress Report," *IGTI Global Gas Turbine News*, May/June, pp. 12–14.
- Suder, K. L., Chima, R. V., Strazisar, A. J., and Roberts, W. B., 1995, "The Effect of Adding Roughness and Thickness to a Transonic Axial Compressor Rotor," *ASME JOURNAL OF TURBOMACHINERY*, Vol. 117, No. 4, pp. 491–505.
- Suder, K. L., 1996, "Experimental Investigation of the Flow Field in a Transonic, Axial Flow Compressor With Respect to the Development of Blockage and Loss," *NASA TM 107310*.
- Suder, K. L., and Celestina, M. L., 1996, "Experimental and Computational Investigation of the Tip Clearance Flow in a Transonic Axial Flow Compressor Rotor," *ASME JOURNAL OF TURBOMACHINERY*, Vol. 118, No. 2, pp. 218–229.